Brief Communications

Stimulation-Evoked Ca^{2+} Signals in Astrocytic Processes at Hippocampal CA3–CA1 Synapses of Adult Mice Are Modulated by Glutamate and ATP

Wannan Tang,[1,3,4] Karolina Szokol,[1,3,6] Vidar Jensen,[1,3] Rune Enger,[1,3,6] Chintan A. Trivedi,[5] Øivind Hvalby,[2] P. Johannes Helm,[3] Loren L. Looger,[7] Rolf Sprengel,[4] and Erlend A. Nagelhus[1,3,6,8]

[1]Centre for Molecular Medicine Norway, The Nordic EMBL Partnership, [2]Department of Physiology, and [3]Letten Centre and GliaLab, Department of Physiology, Institute of Basic Medical Sciences, University of Oslo, 0317 Oslo, Norway, [4]Department of Molecular Neurobiology and [5]Neural Circuits and Behaviour Research Group, Department of Biomedical Optics, Max Planck Institute for Medical Research, D-69120 Heidelberg, Germany, and [6]Oslo University Hospital, Department of Neurology, 0027 Oslo, Norway, [7]Howard Hughes Medical Institute, Janelia Farm Research Campus, Ashburn, Virginia 20147, and [8]Center for Translational Neuromedicine, Department of Neurosurgery, University of Rochester Medical Center, Rochester, New York 14618

To date, it has been difficult to reveal physiological Ca^{2+} events occurring within the fine astrocytic processes of mature animals. The objective of the study was to explore whether neuronal activity evokes astrocytic Ca^{2+} signals at glutamatergic synapses of adult mice. We stimulated the Schaffer collateral/commissural fibers in acute hippocampal slices from adult mice transduced with the genetically encoded Ca^{2+} indicator GCaMP5E driven by the glial fibrillary acidic protein promoter. Two-photon imaging revealed global stimulation-evoked astrocytic Ca^{2+} signals with distinct latencies, rise rates, and amplitudes in fine processes and somata. Specifically, the Ca^{2+} signals in the processes were faster and of higher amplitude than those in the somata. A combination of P2 purinergic and group I/II metabotropic glutamate receptor (mGluR) antagonists reduced the amplitude of the Ca^{2+} transients by 30–40% in both astrocytic compartments. Blockage of the mGluRs alone only modestly reduced the magnitude of the stimulation-evoked Ca^{2+} signals in processes and failed to affect the somatic Ca^{2+} response. Local application of group I or I/II mGluR agonists or adenosine triphosphate (ATP) elicited global astrocytic Ca^{2+} signals that mimicked the stimulation-evoked astrocytic Ca^{2+} responses. We conclude that stimulation-evoked Ca^{2+} signals in astrocytic processes at CA3–CA1 synapses of adult mice (1) differ from those in astrocytic somata and (2) are modulated by glutamate and ATP.

Key words: **astrocytes; endfeet; GCaMP; glia; hippocampus; two-photon**

Introduction

Accumulating evidence suggests that astrocytes respond to synaptic activity by increases in intracellular Ca^{2+} concentration and modulate synaptic transmission and plasticity by Ca^{2+}-dependent release of gliotransmitters (Nedergaard and Verkhratsky, 2012; Araque et al., 2014; Volterra et al., 2014). However, the concept of bidirectional communication between neurons and astrocytes is heavily debated (Agulhon et al., 2010). A central tenet is whether astrocytes in adult animals directly sense synaptic activity. The vast majority of studies on activity-induced astrocytic Ca^{2+} signals have used pups, because bulk loading of membrane-permeable organic Ca^{2+} indicators is most effective in immature animals (Reeves et al., 2011). However, the expression of receptors and neuronal–glial signaling may differ between immature and mature animals. Notably, a recent study demonstrated that the expression of mGluR5 (a group I mGluR) is developmentally regulated, and the authors failed to observe mGluR5-dependent increases in Ca^{2+} levels in cortical astrocytes of adult mice (Sun et al., 2013). That study, as with the vast majority of studies on neuronal–glial signaling, used bulk loading of an organic Ca^{2+} indicator, a strategy that reports mainly on Ca^{2+} signaling events within the cell body and proximal processes, leaving most of the astrocytic territory unsampled (Reeves et al., 2011). Thus, studies using improved Ca^{2+} indicators are needed to resolve whether, and if so how, synaptic activity elicits Ca^{2+} signals within delicate astrocytic processes in adult animals.

We hypothesized that activity at CA3–CA1 hippocampal synapses of adult mice evokes Ca^{2+} signals in fine astrocytic processes

Received Aug. 10, 2014; revised Jan. 6, 2015; accepted Jan. 11, 2015.

Author contributions: W.T., K.S., V.J., R.E., O.H., P.J.H., R.S., and E.A.N. designed research; W.T., K.S., V.J., R.E., and C.A.T. performed research; L.L.L. contributed unpublished reagents/analytic tools; W.T., K.S., and R.E. analyzed data; W.T., R.E., O.H., L.L.L., and E.A.N. wrote the paper.

This work was supported by a European Molecular Biology Organization short-term fellowship (W.T.), the German Academic Exchange Service (DAAD) mobility programme Germany–Norway (R.S. and E.A.N.), the Research Council of Norway (E.A.N.), the European Union Seventh Framework Programme for Research, Technological Development, and Demonstration under Grant Agreement 601055, and the Letten Foundation. We thank Prof. Petter Laake (Department of Biostatistics, Institute of Basic Medical Sciences, University of Oslo, Oslo, Norway) for advice on the statistical analysis.

The authors declare no competing financial interests.

This article is freely available online through the *J Neurosci* Author Open Choice option.

Correspondence should be addressed to either Wannan Tang or Erlend A. Nagelhus, Letten Centre and GliaLab, Department of Physiology, Institute of Basic Medical Sciences, University of Oslo, 0317 Oslo, Norway. E-mail: wannan.tang@medisin.uio.no, e.a.nagelhus@medisin.uio.no.

DOI:10.1523/JNEUROSCI.3319-14.2015

 0270-6474/15/353016-06$15.00/0

by mechanisms involving group I/II mGluRs and P2 purinergic receptors, as observed in astrocytic somata and proximal processes of immature animals (Porter and McCarthy, 1996; Bowser and Khakh, 2004). We took advantage of two-photon microscopy and recombinant adeno-associated virus (rAAV) gene delivery of the genetically encoded Ca^{2+} indicator GCaMP5E and its membrane-tethered version Lck-GCaMP5E (Akerboom et al., 2012), which enable monitoring of Ca^{2+} signals even within distal processes. We report that stimulation of the Schaffer collateral/commissural fibers (Scc) in acute hippocampal slices from adult mice transduced with GCaMP5E driven by the glial fibrillary acidic protein (*GFAP*) promoter elicited robust Ca^{2+} increases within the entire astrocytic territory. However, the kinetics and amplitudes of the stimulation-evoked Ca^{2+} signals differed between astrocytic compartments. Notably, the fastest response almost inevitably occurred in the fine processes, in which it was sensitive to antagonists of both group I/II mGluRs and P2 purinergic receptors.

Materials and Methods

Plasmid constructs. The GCaMP5E (Akerboom et al., 2012) DNA sequence was cloned with BamHI and HindIII into the rAAV vector pAAV–6P–SEWB (Tang et al., 2009) under the human *Synapsin-1* (*SYN*) promoter to generate the construct pAAV–*SYN*–GCaMP5E. The human *GFAP* promoter (Hirrlinger et al., 2009) was inserted with MluI and BamHI into the pAAV–*SYN*–GCaMP5E vector, resulting in the pAAV–*GFAP*–GCaMP5E construct. The Lck sequence ATGGGCTGTG GCTGCAGCTCAAACCCTGAAGATGACTGGATGGAGAACATTGA CGTGTGTGAGAACTGCCATTATCCCC together with 5′-AATTC and 3′-G flanking sequences as overhangs was synthesized and subcloned between EcoRI and BamHI sites of plasmid pAAV–*SYN*–GCaMP5E. The *GFAP* promoter was then cloned with 5′ MluI, 3′ BamHI (from insert), and EcoRI (from vector) with Klenow fill-in into pAAV–*SYN*–GCaMP5E to generate pAAV–*GFAP*–Lck-GCaMP5E.

Virus transduction. rAAV serotypes 1 and 2 were generated as described previously (Tang et al., 2009) and purified by AVB Sepharose affinity chromatography (Smith et al., 2009) after titration with real-time PCR (each titer $\sim 1.0-6.0 \times 10^{12}$ viral genomes/ml; TaqMan Assay; Applied Biosystems). Viruses were stereotactically injected into the brains of deeply anesthetized [mixture of zolazepam (188 mg/kg body weight), tiletamine (188 mg/kg body weight), xylazine (4.5 mg/kg body weight), and fentanyl (26 μg/kg body weight)] 6- to 8-week-old male C57BL/6N mice (Charles River) as described previously (Tang et al., 2009). All procedures were performed according to the guidelines of the local animal use and care committee.

Immunohistochemistry and confocal imaging. The immunohistochemistry and confocal imaging were performed as described previously (Tang et al., 2009; Haj-Yasein et al., 2014) with polyclonal rabbit anti-green fluorescent protein (GFP; 1:3000; catalog #ab6556; Abcam), chicken anti-GFAP (1:1000; catalog #PCK-591P; Covance), rat anti-CD31 (1:200; catalog #550274; BD Biosciences), and FITC-coupled anti-rabbit, Cy3-coupled anti-chicken, and Cy5-coupled anti-rat secondary antibodies (1:200; catalog #711095152, #703165155, and #712175153, respectively; Jackson ImmunoResearch). Image analysis was done with NIH ImageJ (version 10.2).

Electrophysiology and in vitro *two-photon Ca^{2+} imaging.* Experiments were performed on acute hippocampal slices prepared from mice 2–6 weeks after virus transduction. Acute hippocampal slices were prepared as described previously (Haj-Yasein et al., 2014) and kept in artificial cerebrospinal fluid (ACSF, bubbled with 95% O_2/5% CO_2) containing (in mM): 124 NaCl, 2 KCl, 1.25 KH_2PO_4, 2 $MgSO_4$, 2 $CaCl_2$, 26 $NaHCO_3$, and 12 glucose (all from Sigma-Aldrich) at 30 ± 1°C. In some experiments, tetrodotoxin (TTX; 1 μM; Tocris Bioscience), (*RS*)-α-methyl-4-carboxyphenylglycine (MCPG; 1 mM; Tocris Bioscience), pyridoxalphosphate-6-azophenyl-2′,4′-disulfonic acid tetrasodium salt (PPADS; 100 μM; Tocris Bioscience), suramin (100 μM; Tocris Bioscience), or 2-aminoethoxydiphenylborane (2-APB; 100 μM; Tocris Bioscience) was added to the ACSF to block voltage-gated sodium channels (TTX), group I/II mGluRs (MCPG), P2 purinergic receptors (PPADS and suramin), or inositol 1,4,5-trisphosphate (IP_3) receptors (2-APB), respectively. Two glass electrodes filled with ACSF and positioned 100–150 μm from each other in CA1 stratum radiatum served as stimulation and recording electrodes [field EPSP (fEPSP) monitoring], respectively. The synaptic strength was assessed by measuring the slope of the rising phase (volts per second) of the fEPSP. Stimulation trains at 20 Hz for 10 s were applied during all experiments except frequency/duration tests, in which the frequency and duration of the trains varied. For the microinjection experiments, ACSF (as control), (1*S*,3*R*)-1-aminocyclopentane-1,3-dicarboxylic acid (ACPD; 400 μM; Tocris Bioscience), (*S*)-3,5-dihydroxyphenylglycine (DHPG; 100 μM; Tocris Bioscience), (*RS*)-2-chloro-5-hydroxyphenylglycine (CHPG; 300 μM; Tocris Bioscience), or ATP (40 mM; Tocris Bioscience) in ACSF was applied by micropipettes placed into the hippocampal striatum radiatum. GCaMP5E fluorescence was recorded by a two-photon laser scanning microscope (model Ultima; Prairie Technologies) with an XLPLN 25×WMP 1.05 numerical aperture water-immersion objective (Olympus) at 900–910 nm laser pulse using a Chameleon Vision II (Coherent) laser. The continuous wave equivalent of the laser power applied was 15–30 mW, depending on the expression level of the fluorescent indicator. Imaging was performed with 30 s baseline, followed by either electrical stimulations or microinjections of ACSF, ACPD, DHPG, CHPG, or ATP using a PV830 Pneumatic PicoPump (10 psi, 100 ms; World Precision Instruments). The recording was done with either 1 or 4 Hz frame rate, and the images were 512 × 512 or 256 × 256 pixels, respectively.

In vivo *two-photon Ca^{2+} imaging.* Mice transduced with rAAV–*GFAP*–GCaMP5E were prepared for *in vivo* two-photon microscopy as described by Sun et al. (2013), with the following modifications. (1) Isoflurane (2% for surgical procedures, 1.5% during imaging) was used for anesthesia. (2) Buprenorphine (0.15 mg/kg) was injected intraperitoneally before surgery. (3) The craniotomy (2 mm in diameter) was made 2 mm posterior and 1.5 mm to the right of bregma. 4) A blunted 26 gauge needle was used to suction out the cortex and expose the hippocampus. The cavity was subsequently filled with 0.4% agarose in saline and sealed by a coverslip. (5) A glass micropipette containing 400 μM ACPD and 250 μg/ml Texas Red-labeled dextran (Life Technologies) dissolved in ACSF was inserted into the hippocampus through a secondary craniotomy 1 mm mediocaudal to the imaging window. The APCD was delivered by a PV830 Pneumatic PicoPump (10 psi, 100 ms; World Precision Instruments) during continuous imaging with a baseline period of 1 min. GCaMP5E fluorescence was recorded by a two-photon laser scanning microscope (model Ultima IV; Prairie Technologies), as described above.

Imaging analysis. Time series of fluorescence images were imported to Fiji ImageJ, and regions of interest (ROIs) were selected manually based on morphology. Astrocytic cell bodies were identified by their projecting branches and endfeet by their characteristic circular pattern around transversely cut vessels and elongated appearance along obliquely cut vessels. ROIs over processes were chosen at least 5 μm away from the perimeter of the soma. The relative change in fluorescence ($\Delta F/F$) in each ROI, the individual traces, and the histograms were all calculated and plotted by MATLAB (R2011b; MathWorks) with custom-written scripts. Standard deviation (SD) images were generated from time-lapse image recordings by Fiji ImageJ. Mathematical calculations were done in Excel (Microsoft).

Statistical analysis. Statistical analysis was performed using Prism (version 6.0b for Mac OSX; GraphPad Software). Kruskal–Wallis test with Dunn's *post hoc* test was used for comparison between astrocytic somata, processes, and endfeet after Scc stimulation. A two-way ANOVA was performed for comparison of signal amplitudes before and after wash-in of drugs and for comparison of treatment effects in somata and processes. Paired *t* test and Wilcoxon's signed-rank test were also used for comparison before and after drug applications. One-sample *t* test was used for comparison of response latencies of the earliest activated processes and the soma.

Results

Viral transduction yields GCaMP5E expression in adult mouse astrocytes

To reveal astrocytic Ca^{2+} signals within the fine astrocytic processes in adult mice, GCaMP5E (Akerboom et al., 2012) was cloned into an rAAV vector and driven by the *GFAP* promoter (Fig. 1*A*), similar to an approach used for GCaMP3 in recent confocal microscopy studies (Shigetomi et al., 2013; Haustein et al., 2014). Three weeks after rAAV injection into the dorsal hippocampus of adult mice, immunohistochemistry of acute hippocampal slices showed successful rAAV-mediated GCaMP5E delivery into astrocytes (Fig. 1*A*). Antibodies against GFP confirmed GCaMP5E expression in GFAP-immunopositive astrocytes, including their fine processes and endfeet adjacent to CD31-immunopositive blood vessels (Fig. 1*A*).

Neuronal activity triggers Ca^{2+} signals within entire astrocytic territories

Stimulation (20 Hz, 10 s) of Scc in acute hippocampal slices from rAAV–*GFAP*–GCaMP5E-transduced animals (Fig. 1*B*) consistently elicited global Ca^{2+} rises in the majority of stratum radiatum astrocytes (Fig. 1*C–E*), mimicking the Ca^{2+} response of CA3 stratum lucidum astrocytes to bursts of mossy fiber action potentials (Haustein et al., 2014). The Ca^{2+} signals, detected by two-photon imaging, occurred along the pathway of the stimulated axons and were rarely observed in stratum pyramidale (Fig. 1*C–E*). The amplitude of the somatic Ca^{2+} transients depended on stimulation frequency and duration, with the maximum response observed at 20 Hz stimulation (Fig. 1*F*). To verify that the Ca^{2+} signals depended on the presence of action potentials, we applied TTX (1 μM), which abolished fEPSPs and the stimulation-evoked astrocytic Ca^{2+} responses (Fig. 1*G*).

Stimulation (20 Hz, 10 s) of Scc increased GCaMP5E fluorescence within all astrocytic compartments in stratum radiatum (Fig. 1*H*). When values from fine processes at different locations within the astrocytic territory were pooled, the latencies of the responses were similar in somata, fine processes, and endfeet, all ~3 s (Fig. 1*I*; image acquisition at 4 Hz). However, in 13 of 16 cells, the fastest Ca^{2+} response occurred in the fine processes. On average, the somatic response lagged ~1 s behind the fastest responding process (Fig. 1*I*). Moreover, the Ca^{2+} transients in the fine processes exhibited a faster rise and higher amplitudes than those in the somata, whereas the duration of the signals was similar in all astrocytic compartments (Fig. 1*I*). In astrocytes expressing viral Lck-GCaMP5E, the membrane-tethered version of GCaMP5E (cf. Shigetomi et al., 2013), the response latency and duration did not differ significantly between compartments (Fig. 1*J–L*). However, the processes exhibited faster rate of rise than somata and endfeet and higher amplitude than the endfeet (Fig. 1*K*,*L*).

Activity-induced Ca^{2+} signals in the fine astrocytic processes are dependent on group I/II mGluRs and P2 purinergic receptors

Because group I/II mGluRs and P2 purinergic receptors have been implicated in stimulation-evoked astrocytic Ca^{2+} signals in pups (Porter and McCarthy, 1996; Bowser and Khakh, 2004), we investigated whether similar responses were seen in adult mice. For all pharmacological studies, we used cytosolic GCaMP5E, which reveals astrocytic somata and endfeet better than Lck-GCaMP5E. Micropipette delivery of the group I/II mGluR agonist ACPD (400 μM) into stratum radiatum elicited a brisk increase in GCaMP5E fluorescence in astrocytic somata, fine processes, and endfeet, mimicking the response to axonal stimulation (Fig. 2*A*). Because astrocytes *in vitro* may differ from astrocytes *in vivo* (Takano et al., 2014), we microinjected ACPD into the hippocampus of rAAV–*GFAP*–GCaMP5E-transduced living mice. Indeed, ACPD (400 μM) also evoked a robust increase in astrocytic GCaMP5E fluorescence *in vivo* (Fig. 2*B*). Next, we applied selective agonists to acute hippocampal slices to determine the mGluR subtype(s) that are implicated in astrocyte activation. Microinjection of the group I mGluR agonist DHPG (100 μM) to stratum radiatum elicited similar astrocytic Ca^{2+} signals as ACPD (Fig. 2*C*), whereas the mGluR5-selective agonist CHPG (300 μM) failed to evoke responses (Fig. 2*D*).

Stimulation (20 Hz, 10 s) of Scc in the presence of the group I/II mGluR antagonist MCPG (1 mM) yielded fEPSP slopes comparable with control conditions (Fig. 2*E*). A two-way ANOVA failed to reveal an effect of MCPG on stimulation-evoked Ca^{2+} signal amplitudes ($p = 0.19$, $F_{(1,138)} = 1.771$), whereas the Wilcoxon's signed-rank test (paired statistical analysis) showed a statistically significant reduction of the amplitude only in the processes (Fig. 2*E*; $p = 0.02$ for processes, $p = 0.08$ for somata).

Application of ATP (40 mM) into the stratum radiatum also evoked brisk Ca^{2+} transients in all astrocytic compartments (Fig. 2*F*). Similar to what we observed after stimulation of Scc, the ATP-induced Ca^{2+} rises showed bigger amplitudes in the fine processes than in the somata (Fig. 2*F*). Activation of Scc in the presence of the nonselective P2 antagonists PPADS (100 μM) and suramin (100 μM) reduced the amplitude of the astrocytic Ca^{2+} responses in fine processes and somata, despite an increase in the fEPSP slope (Fig. 2*G*; two-way ANOVA, $p < 0.005$, $F_{(1, 280)} = 13.76$). Application of MCPG together with PPADS and suramin had a similar effect on the Ca^{2+} signal amplitudes as PPADS and suramin (Fig. 2*H*; the triple drug combination reduced amplitudes in processes and somata by 40 and 28%, respectively; two-way ANOVA, $p < 0.001$, $F_{(1, 158)} = 37.29$). However, the amplitude reductions were not significantly different between the two compartments (two-way ANOVA, $p = 0.21$, $F_{(1, 219)} = 1.55$).

Activity-induced astrocytic Ca^{2+} transients are dependent on IP_3 receptor-mediated Ca^{2+} release from internal stores

To explore whether the astrocytic Ca^{2+} signals were dependent on IP_3 receptor-mediated Ca^{2+} release from internal stores, we applied the membrane-permeable IP_3 receptor antagonist 2-APB (100 μM). 2-APB did not affect fEPSP slope but strongly suppressed stimulation-evoked astrocytic Ca^{2+} transients occurring within 15 s after stimulation (Fig. 2*I*,*J*). In addition, in four of eight slices, delayed astrocytic Ca^{2+} signals (>15 s) were observed (Fig. 2*I*).

Discussion

Our study shows that stratum radiatum astrocytes of adult mice are able to elicit intracellular Ca^{2+} signals in response to neuronal activity. The latencies of the responses were 2–3 s, mimicking the sensory-evoked Ca^{2+} responses in cortical astrocytes *in vivo* (Wang et al., 2006). Sub-second responses, as observed in a minority of cortical astrocytes *in vivo* (Winship et al., 2007), were not detected in our experiments.

We found that the fastest Ca^{2+} response usually occurred within the fine astrocytic processes, on average ~1 s before detectable soma activity. This finding may depend on the shorter diffusion distance of synaptically released mediators to the perisynaptic astrocytic membrane. The stimulation-evoked Ca^{2+} signals in the fine astrocytic processes also differed from those in astrocytic somata in having faster rate of rise and amplitude, both

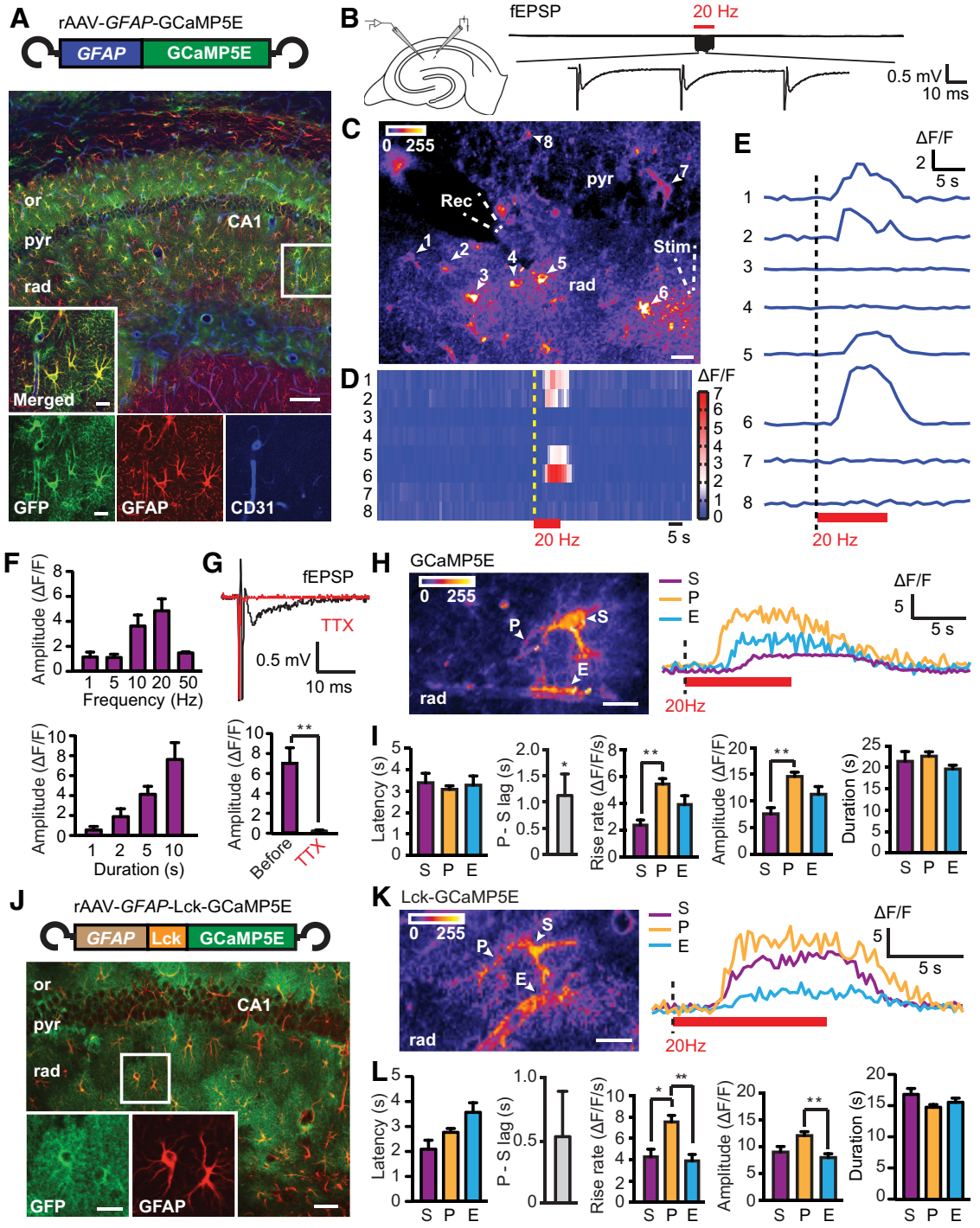

Figure 1. Stimulation-evoked Ca^{2+} signals in astrocytic territories of adult mice monitored by two-photon GCaMP5E imaging. ***A***, Viral (rAAV) transduction of GCaMP5E driven by *GFAP* promoter in adult mouse hippocampus. Immunofluorescence with GFP antibodies (green) shows robust GCaMP5E expression in GFAP-immunopositive (red) CA1 astrocytes. The vascular endothelium is revealed with CD31 antibodies (blue). or, Stratum oriens; pyr, stratum pyramidale; rad, stratum radiatum. Scale bars: 100 and 10 μm (boxed motif expanded in inset). ***B***, Schematic drawing of electrode placements in the hippocampal slice and fEPSPs recorded during a 20 Hz stimulation train expanded in the bottom trace. ***C***, SD image of fluorescence intensities from a time-lapse recording at 1 Hz frame rate. The positions of GCaMP5E fluorescent astrocytic somata (1–8) and electrodes are indicated. Rec, recording; Stim, stimulation. Scale bar, 20 μm. ***D***, Activity histogram ($\Delta F/F$) of astrocytic somata 1–8. Red bar indicates electrical Scc stimulation. ***E***, Single GCaMP5E fluorescence traces from somata of astrocytes 1–8 during activation. ***F***, Amplitudes of the somatic Ca^{2+} signals in response to 10 s stimulation with different frequencies (top) and at 20 Hz stimulation with different durations (bottom). ***G***, TTX abolished stimulation-evoked astrocytic Ca^{2+} responses (paired *t* test, $n = 11$ cells, 4 slices from 3 animals). ***H***, SD image of fluorescence intensities from rAAV–*GFAP*–GCaMP5E-transduced hippocampal striatum radiatum astrocyte (4 Hz frame rate), in which soma (S), process (P), and endfeet (E) are indicated. Scale bar, 10 μm. ***I***, Latency, rise rate, amplitude, and duration of stimulation-evoked (20 Hz, 10 s) GCaMP5E fluorescence responses in astrocytic somata, processes, and endfeet (abbreviations as above). P-S lag indicates the time between the first response occurring in fine process and the somatic response. This lag analysis was performed by one-sample *t* test, $n = 16$ cells with paired observations. Other comparisons were done by Kruskal–Wallis test with Dunn's *post hoc* test, $n = 23$ (somata), 99 (processes), and 26 (endfeet), 7 slices from 3 animals. ***J***, As in ***A*** but with transduction of Lck-GCaMP5E instead of GCaMP5E. Scale bars: low magnification, 50 μm; high magnification, 10 μm. ***K***, As in ***H*** but with rAAV–*GFAP*–Lck-GCaMP5E. ***L***, As in ***I*** but with rAAV–*GFAP*–Lck-GCaMP5E, $n = 21$ (somata), 106 (processes), and 32 (endfeet), 8 slices from 2 animals; $n = 18$ cells for the lag analysis. Values are mean ± SEM. $^*p < 0.05$, $^{**}p < 0.001$.

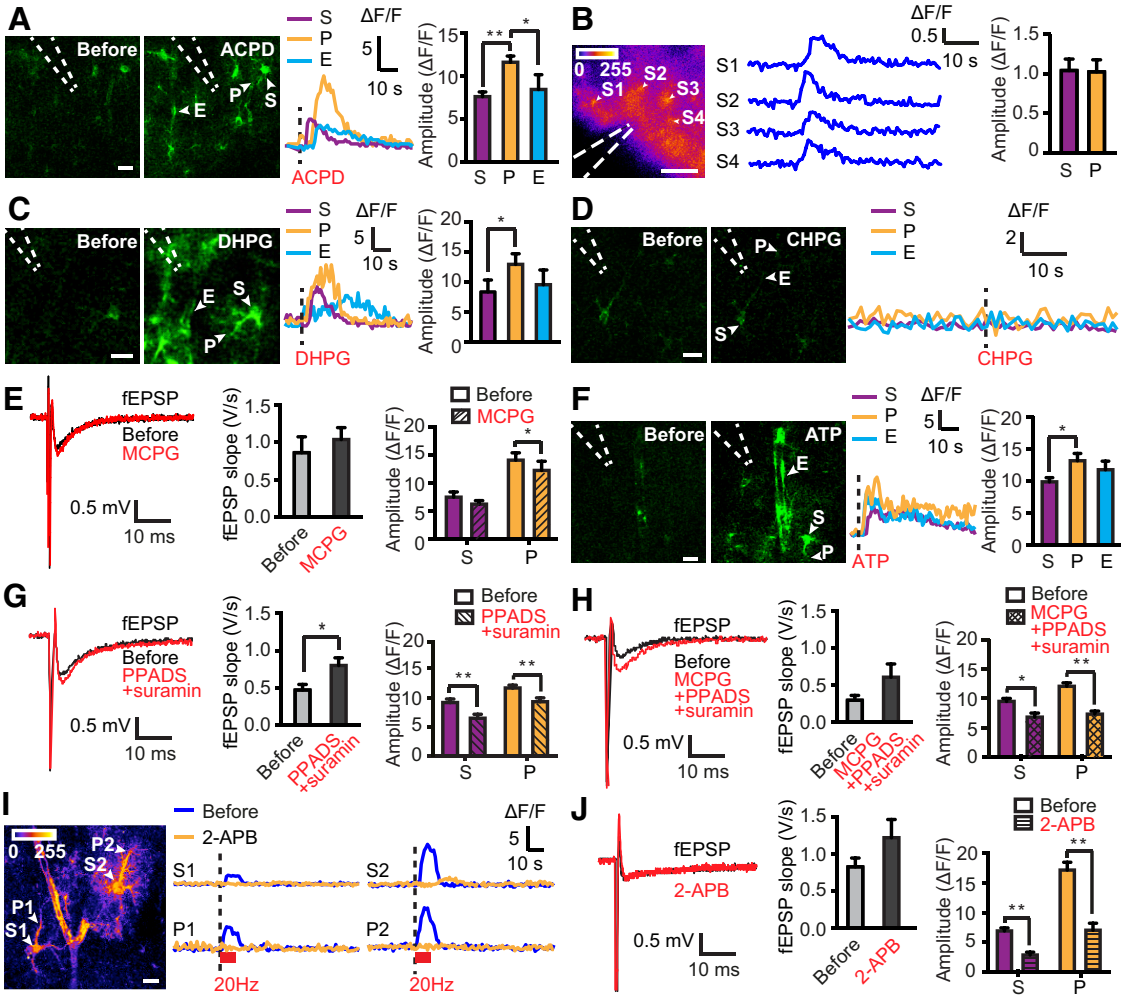

Figure 2. Astrocytic Ca^{2+} signals depend on mGluRs and purinergic receptors. ***A***, Images of GCaMP5E fluorescence before and after ACPD delivery through a micropipette (dashed lines) into the acute hippocampal slice preparation. Scale bar, 10 μm. The fluorescence traces are from the astrocytic soma (S), process (P), and endfoot (E) as indicated. Bar diagram shows amplitudes [Kruskal–Wallis test with Dunn's *post hoc* test, $n = 67$ (somata), 86 (processes), and 20 (endfeet), 7 slices from 3 animals]. ***B***, Astrocytic GCaMP5E fluorescence responses to ACPD microinjected into the hippocampus *in vivo*. SD image of fluorescent intensities (left) and individual traces (middle) of $\Delta F/F$ from astrocytic somata (S1–S4) during ACPD application (1 Hz frame rate). Dashed lines indicate position of delivery pipette. Scale bar, 100 μm. Right, Quantification of amplitude of ACPD-evoked astrocytic Ca^{2+} responses in somata (S) and processes (P) [unpaired *t* test, $n = 32$ (somata) and 25 (processes), 9 trials in 4 animals]. ***C***, As in ***A*** but with DHPG [$n = 30$ (somata), 35 (processes), and 16 (endfeet), 8 slices from 4 animals]. ***D***, Microinjection of CHPG into acute hippocampal slices failed to elicit astrocytic GCaMP5E fluorescence responses in five slices from four mice (16 somata, 25 processes, and 4 endfeet were analyzed). Shown are example traces before and after microinjection. Scale bar, 10 μm. ***E***, Example fEPSPs and mean fEPSP slopes and astrocytic GCaMP5E fluorescence transients elicited by Scc stimulation before and after application of MCPG to the slice solution. Two-way ANOVA failed to reveal an effect of MCPG on Ca^{2+} signal amplitude, whereas the Wilcoxon's signed-rank test showed a significant amplitude reduction in astrocytic processes (P) ($n = 34$) but not in somata (S) ($n = 37$; 7 slices from 4 animals). ***F***, As in ***A*** but with ATP [$n = 36$ (somata), 35 (processes), and 19 (endfeet), 3 slices from 2 animals]. ***G***, As in ***E*** but with PPADS and suramin [$n = 50$ (somata) and 92 (processes), 10 slices from 6 animals]. ***H***, As in ***E*** but with a mixture of MCPG, PPADS, and suramin [$n = 30$ (somata) and 51 (processes), 7 slices from 4 animals]. ***I***, Baseline SD image of fluorescence intensities (1 Hz frame rate). Scale bar, 10 μm. Individual traces from somata and processes during 2-APB application. ***J***, As in ***E*** but with 2-APB [$n = 41$ (somata) and 38 (processes), 8 slices from 4 animals; only transients with peak amplitude within 15 s after Scc stimulation are included]. Values are mean ± SEM. $^*p < 0.05$, $^{**}p < 0.001$.

of which may rely on the larger surface/volume ratio of processes. Inhibition of group I/II mGluRs with MCPG only modestly reduced the Ca^{2+} transient amplitude in astrocytic processes and did not exert a statistically significant effect in somata. Thus, the effect of group I/II mGluR blockage on astrocytic Ca^{2+} signals in adult mice was much less prominent than what was reported in rat pups (Porter and McCarthy, 1996), consistent with the observation that mGluR5 expression is developmentally regulated (Sun et al., 2013). Indeed, we were unable to elicit astrocytic Ca^{2+} transients with the selective mGluR5 agonist CHPG in the adult hippocampus. However, application of DHPG, an agonist of group I mGluRs (i.e., mGluR1 and mGluR5), evoked a response that mimicked that of the group I/II mGluR agonist ACPD. Together, our findings suggest a role for mGluR1 receptors in modulating the stimulation-evoked astrocytic Ca^{2+} transients.

In line with previous observations in pups (Bowser and Khakh, 2004; Petravicz et al., 2008), our data revealed that astrocytic Ca^{2+} signals in response to Scc stimulation are dependent on P2 purinergic receptors and IP_3 receptor-mediated Ca^{2+} release from internal stores. The combined blockage of group I/II mGluRs and P2 purinergic receptors reduced peak Ca^{2+} amplitude by ~30–40%.

Using confocal microscopy on acute hippocampal slices, Haustein et al. (2014) recently explored astrocytic Ca^{2+} signals during activation of the mossy fiber CA3 pyramidal cell pathway and concluded that the signals were primarily mediated by mGluR2/3 and $GABA_B$ receptors. That study applied various

drugs in combination with mGluR2/3 inhibition and failed to detect an effect of $P2Y_1$ receptor blockage.

Synaptic properties at the mossy fiber/CA3 synapses are very different from those at the small CA3–CA1 synapses. For instance, the stimulation frequency (1–15 Hz) applied in the mossy fiber system would evoke a many-fold increase in glutamate response compared with a similarly applied stimulation regimen at CA1 synapses. Type and distribution of mGluRs and their pharmacological profiles may also differ significantly (Henze et al., 2000).

In contrast to Haustein et al. (2014), we also provide evidence that action potential-evoked Ca^{2+} signals within the astrocytic territory differ in amplitude and kinetics, with the fastest response occurring in astrocytic processes. Studies using other pharmacological approaches, gene knock-out, or optogenetics are likely to provide additional insight into the complex mechanisms underlying astrocyte sensation of neuronal activity. Diversity of neural activity-evoked Ca^{2+} signals must be accounted for when probing astrocyte function in neural circuits.

References

Agulhon C, Fiacco TA, McCarthy KD (2010) Hippocampal short- and long-term plasticity are not modulated by astrotyte Ca2+ signaling. Science 327:1250–1254. Medline

Akerboom J, Chen TW, Wardill TJ, Tian L, Marvin JS, Mutlu S, Calderón NC, Esposti F, Borghuis BG, Sun XR, Gordus A, Orger MB, Portugues R, Engert F, Macklin JJ, Filosa A, Aggarwal A, Kerr RA, Takagi R, Kracun S, Shigetomi E, Khakh BS, Baier H, Lagnado L, Wang SS, Bargmann CI, Kimmel BE, Jayaraman V, Svoboda K, Kim DS, Schreiter ER, Looger LL (2012) Optimization of a GCaMP calcium indicator for neural activity imaging. J Neurosci 32:13819–13840. Medline

Araque A, Carmignoto G, Haydon PG, Oliet SH, Robitaille R, Volterra A (2014) Gliotransmitters travel in time and space. Neuron 81:728–739. Medline

Bowser DN, Khakh BS (2004) ATP excites interneurons and astrocytes to increase synaptic inhibition in neuronal networks. J Neurosci 24:8606–8620. Medline

Haj-Yasein NN, Bugge CE, Jensen V, Ostby I, Ottersen OP, Hvalby O, Nagelhus EA (2014) Deletion of aquaporin-4 increases extracellular K+ concentration during synaptic stimulation in mouse hippocampus. Brain Struct Funct. Advance online publication. Retrieved January 14, 2015. doi:10.1007/s00429-014-0767-z. CrossRef Medline

Haustein MD, Kracun S, Lu XH, Shih T, Jackson-Weaver O, Tong X, Xu J, Yang XW, O'Dell TJ, Marvin JS, Ellisman MH, Bushong EA, Looger LL, Khakh BS (2014) Conditions and constraints for astrocyte calcium signaling in the hippocampal mossy fiber pathway. Neuron 82:413–429. Medline

Henze DA, Urban NN, Barrionuevo G (2000) The multifarious hippocampal mossy fiber pathway: a review. Neuroscience 98:407–427. Medline

Hirrlinger J, Scheller A, Hirrlinger PG, Kellert B, Tang W, Wehr MC, Goebbels S, Reichenbach A, Sprengel R, Rossner MJ, Kirchhoff F (2009) Split-cre complementation indicates coincident activity of different genes in vivo. PLoS One 4:e4286. Medline

Nedergaard M, Verkhratsky A (2012) Artifact versus reality–how astrocytes contribute to synaptic events. Glia 60:1013–1023. Medline

Petravicz J, Fiacco TA, McCarthy KD (2008) Loss of IP3 receptor-dependent Ca2+ increases in hippocampal astrocytes does not affect baseline CA1 pyramidal neuron synaptic activity. J Neurosci 28:4967–4973. Medline

Porter JT, McCarthy KD (1996) Hippocampal astrocytes in situ respond to glutamate released from synaptic terminals. J Neurosci 16:5073–5081. Medline

Reeves AM, Shigetomi E, Khakh BS (2011) Bulk loading of calcium indicator dyes to study astrocyte physiology: key limitations and improvements using morphological maps. J Neurosci 31:9353–9358. Medline

Shigetomi E, Bushong EA, Haustein MD, Tong X, Jackson-Weaver O, Kracun S, Xu J, Sofroniew MV, Ellisman MH, Khakh BS (2013) Imaging calcium microdomains within entire astrocyte territories and endfeet with GCaMPs expressed using adeno-associated viruses. J Gen Physiol 141:633–647. Medline

Smith RH, Levy JR, Kotin RM (2009) A simplified baculovirus-AAV expression vector system coupled with one-step affinity purification yields high-titer rAAV stocks from insect cells. Mol Ther 17:1888–1896. Medline

Sun W, McConnell E, Pare JF, Xu Q, Chen M, Peng W, Lovatt D, Han X, Smith Y, Nedergaard M (2013) Glutamate-dependent neuroglial calcium signaling differs between young and adult brain. Science 339:197–200. Medline

Takano T, He W, Han X, Wang F, Xu Q, Wang X, Oberheim Bush NA, Cruz N, Dienel GA, Nedergaard M (2014) Rapid manifestation of reactive astrogliosis in acute hippocampal brain slices. Glia 62:78–95. Medline

Tang W, Ehrlich I, Wolff SB, Michalski AM, Wölfl S, Hasan MT, Lüthi A, Sprengel R (2009) Faithful expression of multiple proteins via 2A-peptide self-processing: a versatile and reliable method for manipulating brain circuits. J Neurosci 29:8621–8629. Medline

Volterra A, Liaudet N, Savtchouk I (2014) Astrocyte Ca^{2+} signalling: an unexpected complexity. Nat Rev Neurosci 15:327–335. Medline

Wang X, Lou N, Xu Q, Tian GF, Peng WG, Han X, Kang J, Takano T, Nedergaard M (2006) Astrocytic Ca2+ signaling evoked by sensory stimulation in vivo. Nat Neurosci 9:816–823. Medline

Winship IR, Plaa N, Murphy TH (2007) Rapid astrocyte calcium signals correlate with neuronal activity and onset of the hemodynamic response *in vivo*. J Neurosci 27:6268–6272. Medline